

Nanoscale

Accepted Manuscript



This is an *Accepted Manuscript*, which has been through the Royal Society of Chemistry peer review process and has been accepted for publication.

Accepted Manuscripts are published online shortly after acceptance, before technical editing, formatting and proof reading. Using this free service, authors can make their results available to the community, in citable form, before we publish the edited article. We will replace this *Accepted Manuscript* with the edited and formatted *Advance Article* as soon as it is available.

You can find more information about *Accepted Manuscripts* in the [Information for Authors](#).

Please note that technical editing may introduce minor changes to the text and/or graphics, which may alter content. The journal's standard [Terms & Conditions](#) and the [Ethical guidelines](#) still apply. In no event shall the Royal Society of Chemistry be held responsible for any errors or omissions in this *Accepted Manuscript* or any consequences arising from the use of any information it contains.

ARTICLE

Mapping Viscoelastic properties of healthy and pathological red blood cells at the nanoscale level

5
G Ciasca^a, M Papi^{a*}, S Di Claudio^a, M Chiarpotto^a, V Palmieri^a, G Maulucci^a, G Nocca^b, C Rossi^b, M De Spirito^a

Abstract In order to pass through the microcirculation red blood cells (RBCs) need to undergo extensive deformations and 10 to recover the original shape. This extreme deformability is altered by various pathological conditions. On the other hand, an altered RBC deformability can have major effects on blood flow and can lead to pathological implications. The study of the viscoelastic response of red blood cells to mechanical stimuli is crucial to fully understand deformability changes under pathological conditions. However, the typical erythrocyte biconcave shape hints to a complex and intrinsically heterogeneous mechanical response that must be investigated by using probes at the nanoscale level. In this work, the local 15 viscoelastic behaviour of healthy and pathological red blood cells was probed by Atomic Force Microscopy (AFM). Our results clearly show that RBC stiffness is not spatially homogeneous, suggesting a strong correlation with the erythrocyte biconcave shape. Moreover, our nanoscale mapping highlights the key role played by viscous forces, demonstrating that RBCs do not behave as a pure elastic body. The fundamental role played by viscous forces is further strengthened by the comparison between healthy and pathological (diabetes mellitus) RBCs. It is well known that pathological RBCs are usually 20 stiffer than healthy ones. Our measures unveil a more complex scenario according to which the difference between normal and pathological red blood cells does not merely lies in stiffness but also in a different dynamical response to external stimuli that is governed by viscous forces.

25 Introduction

In physiological conditions, RBCs undergo repeated severe deformations when travelling through small blood vessels and organs¹. This remarkable deformability is closely related 30 to RBC membrane structure, primarily consisting of a phospholipid bilayer with an underlying two-dimensional network of spectrin molecules²⁻⁷. The composite RBC membrane is responsible for discoid shape of healthy RBCs and their elastic properties. The lipid bilayer mainly 35 contributes to bending resistance and maintains the cells surface area, while spectrin network has shear elastic properties⁶.

A reduced RBC deformability is known to be related to several pathological conditions, such as diabetes mellitus,

40 essential hypertension, arteriosclerosis and coronary artery, and to be responsible for an enhanced flow resistance of blood^{1, 4, 8-13}.

RBCs are very sensitive to the capillary flow velocity and are able to modify as a result their shape. The critical flow 45 velocities of the RBCs shape transitions are linearly dependent on their elastic proprieties and, since the hematocrit of normal human blood is about 45%, even little RBC mechanical modifications can lead to a dramatic increase of blood flow resistance¹⁴.

50 For these reasons RBCs bio-mechanical properties have been extensively studied by various techniques: micropipette aspiration, filtration based methods, laser diffractoscopy, microchannel method and atomic force microscopy (AFM)^{6, 15-19}.

In this context, one of the major properties to look quantitatively at red blood cell stiffness is the Young's modulus (E) as measured by AFM through the recording of force-distance curves²⁰.

5 Several AFM works pointed out a strong correlation between erythrocytes stiffness and the presence of selected pathology. Very recently Pretorius and coworkers showed that erythrocyte extracted from high serum ferritin level Alzheimer's Disease (AD) patients have an increased 10 Young's modulus with respect to healthy and normoferritinemic AD control patients²⁰, providing a further confirmation of the strength relation between AD and ferritin²¹. Dulinska et al. showed that the erythrocyte stiffness in blood samples taken from hereditary 15 spherocytosis, thalassemia and G6PD deficiency are larger than that obtained from the healthy control group¹⁰. Fornal et al pointed out that the average Young's modulus in diabetic patients exceeds that for healthy persons by a factor greater than 3²². Similarly, Lykotrafitis and coworkers demonstrated 20 that Sicke-cells disease RBCs are stiffer than the control ones¹.

This large body of experimental evidence showing a stiffness increase in pathological RBCs, opened the way to the development of novel RBC-related biomechanical 25 markers of disease.

In the present work, stiffness of normal and pathological erythrocytes was measured by AFM in physiological conditions. In particular AFM was used to map the local variation of RBC Young's modulus with a spatial resolution 30 down to few hundreds of nanometers. The viscoelastic behavior of healthy and pathological red blood cells was also investigated pointing out the key role played viscous by forces

35 Material and methods

Human whole blood was obtained from healthy donors volunteers (15 subjects) and diabetes mellitus II patients (5 subjects), anticoagulated with heparin and centrifuged to separate blood form serum. Blood was obtained by 40 venipuncture at the Policlinico Gemelli of Rome in accordance with the institutional bioethics code. In order to probe mechanical properties of red blood cells by AFM, erythrocytes were resuspended in 10 mM phosphate buffered saline (PBS, 150 mM NaCl, 27 mM KCl, pH = 7.4, from 45 Sigma) and deposited on a poly-l-lysine coated petri dish. After 1-hour incubation, the poly-l-lysine coated petri dish was gently washed in PBS to remove unattached red blood cells. During experiments RBCs were kept at the constant temperature of 37°C.

50 Atomic force microscopy was performed in liquid environment using a JPK Nanowizard II atomic force microscope (JPK instruments, Berlin Germany) coupled to an optical microscope (Axio observer, Carl Zeiss, Milan, Italy). MikroMash silicon cantilevers with a spring constant 55 of approximately 0.05 N/m and a tip radius of about 10 nm were used (CSC38, MikroMash). The cantilever spring constant was computed for each measurement by thermal calibration and the half opening angle of tip apex was accurately determined by electron microscopy. Force curves 60 were acquired by using an indentation force of 0.5 nN at different indentation rates in the range 0.5-25 $\mu\text{m/s}$.

10 different cells were measured for each of the subjects. Cells were chosen by using

ARTICLE

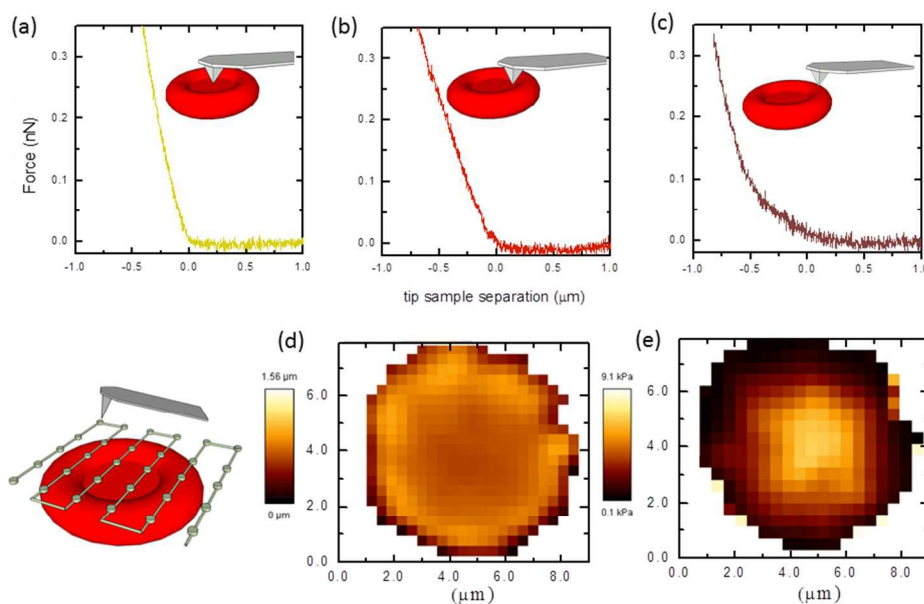


Figure 1: (panel 1-c) representative force-distance curves acquired at different distance from the red blood cells centre. Cantilever position is schematically represented in the figures insets; (panel d) nanoscale zero force image of the entire erythrocyte; (panel e) nanoscale Young's modulus map of the entire erythrocyte.

optical microscope images, as discussed in the supplementary information (fig. S1).

Indentation curves were analyzed by using the modified Hertzian model developed in ref^{23,24} for conical indenters.

5

$$F(\delta) = \frac{2E \tan(\alpha)}{\pi(1-\nu^2)} \delta^2 \quad (1)$$

where E accounts for the apparent Young's modulus, ν for the Poisson ratio and δ for the indentation depth. The Poisson ratio was set at 0.5 to account for material incompressibility. An indentation range of 0 – 200 nm was analyzed, as in this range, the infinitesimal strain model is considered still valid^{25,26}.

The local biomechanical response of erythrocytes was investigated by mapping the apparent Young's modulus E retrieved by using eq. 1²⁷⁻²⁹. Maps size was generally 8 x 8 μm. Different resolutions were adopted, depending on the indentation rate. 32 x 32 pixels maps that correspond to a spatial resolution of about 250 nm were acquired for an indentation rate of 5 μm/s. 8 x 8 pixels maps (about 1 μm

spatial resolution) were acquired for other indentation rates.

Typical acquisition times were approximately 90 minutes for 32 x 32 pixels maps and 10 minutes for 8 x 8 pixels maps when an indentation rate of 5 μm/s is adopted. Lower/higher indentation rate requires lower/higher acquisition time.

25

The same fitting procedure used to measure Young's modulus allows for the contemporaneous determination of the AFM tip contact-point offset. The three dimensional shape of red blood cells was indeed investigated by the recovery of its zero-force image obtained by mapping the contact point off-set. The zero force image provides direct information on the RBC topology and, at the same time, minimizes the effect of shape modifications, e.g. heights compression, induced by the applied force in the conventional AFM imaging mode³⁰.

35

The role played by viscous forces in the biomechanical response of red blood cells was qualitatively evaluated

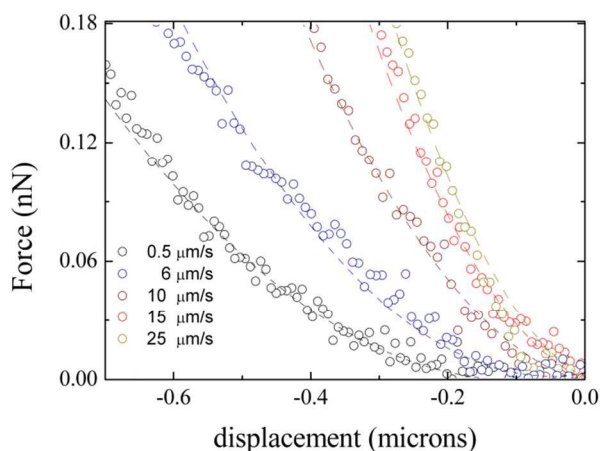


figure 2: force distance curves acquired at different indentation rates on the same cell .

by studying the dependence of E by the indentation rate. To evaluate also quantitatively the contribution of dissipative forces, we estimated the energy dissipated during the deformation process (or Hysteresis H). H was computed as the difference between the area (A_e) under the approach curve ($F_e(d)$) and that (A_r) under the retract curve ($F_r(d)$) normalized by A_e ³¹:

$$H = \frac{\int_0^\delta F_E(\delta) d\delta - \int_0^\delta F_R(\delta) d\delta}{\int_0^\delta F_E(\delta) d\delta} = \frac{A_E - A_R}{A_E} \quad (2)$$

10 Results and discussion

Nanoscale mapping of Young's modulus distribution of normal red blood cells

In fig. 1 a-c three indentation curves acquired at different distances from the RBC centre are shown. Cantilever position is schematically represented in figure insets. Measures were acquired using an indentation rate of 5 $\mu\text{m/s}$. Force-distance curves appear to be qualitatively different moving from cell periphery to the centre, unveiling a not homogeneous Young's modulus spatial distribution. This behavior suggests that a single point measure could not be representative of the whole cell mechanical response. Therefore we decided to probe the local response of RBCs by acquiring force-distance curves at different positions over the cell surfaces, as schematically represented in fig. 1 (lower left corner). A representative erythrocyte characterized by an average E value close to that measured on the whole group of subjects was chosen. Fig. 1d and 1e

show two nanoscale maps of the entire RBC acquired with a spatial resolution of about 250 nm. Fig. 1d shows a zero-force image of the erythrocyte, obtained as described in materials and methods. The typical biconcave shape of healthy RBCs is clearly observable. Fig 1e shows the corresponding E values obtained by fitting equation 1 to experimental curves. The RBC appears to be stiffer in its centre and softer at the cell periphery. The average measured Young's Modulus over the whole red blood cell surface was 1.87 ± 0.90 kPa. The highest measured E value is about 9 kPa, the lowest is about 60 Pa. Interestingly, the comparison between the two maps highlights an evident inverse correlation between RBCs topology and stiffness. A similar behavior was detected in the other cells extracted from different healthy subjects (see fig S2 and S3 in the supplementary informations)

An average value of 1.82 ± 0.20 kPa with a standard deviation of 1.6 kPa was measured over the whole group of healthy subjects. This value is similar to that recently measured in ref¹² where a E of 1.81 ± 0.44 kPa was obtained by pooling about 40 blood samples. A detailed comparison with the average value measured in the present work and in similar experimental works^{1, 4, 8, 10-13} is reported in tab. S1 in the supplementary information.

Relevance of viscous forces in the mechanical response of healthy red blood cells.

In figure 2 a representative set of force-distance curves performed at different indentation rates and acquired on a RBC extracted from a healthy donor are shown. By increasing indentation rate an increase in the reaction force is observed. This evidence suggests that RBCs do not behave as pure elastic bodies; conversely dissipative forces play a relevant role in determining their mechanical response.

Given the heterogeneous and local nature of the mechanical response of RBCs shown in fig 1, we acquired several maps at different indentation rates. A spatial resolution of about 1 micron was chosen to avoid extensive sample drift occurring especially at low indentation rates, where the acquisition time is increased.

In figure 3 a set of selected maps acquired at different indentation rates are reported. The same color scale was used for all maps. Even though the lower resolution, a Young's

ARTICLE

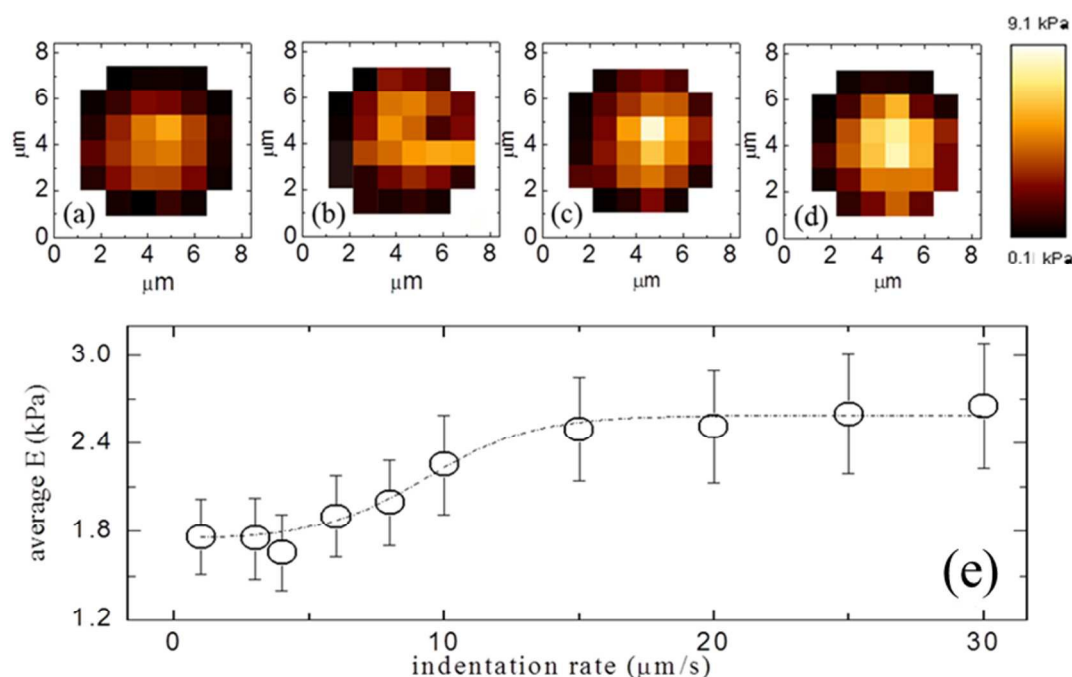


Figure 3: set of representative Young's modulus maps acquired at different indentation rates, namely $1\mu\text{m/s}$ (panel a); $6\mu\text{m/s}$ (panel b), $10\mu\text{m/s}$ (panel c), $20\mu\text{m/s}$ (panel d). Average Young's modulus E as a function of the indentation rate. A sigmoidal curve was fitted to data (dotted line). Error bars correspond to the standard deviation of the mean computed over all the measured cells.

modulus distribution similar to that shown in fig. 1 can be observed: RBC appears stiffer in its center than in its periphery, independently from the indentation rate. By increasing indentation rate, maps appear brighter pointing out a global increase in RBC stiffness. In fig 3 we reported the average E computed by taking into account all maps acquired on the control group. Up to reach $5\mu\text{m/s}$, E assumes a constant value of about 1.8 kPa . After $5\mu\text{m/s}$, E starts increasing up to reach a plateau value of about 2.5 kPa at $15\mu\text{m/s}$. This behavior confirms the preponderant role of the viscous force in determining the mechanical response of erythrocytes.

To evaluate quantitatively the contribution of dissipative forces, we estimated the energy dissipated during the deformation process (or Hysteresis H). H was computed for different indentation rates as described in material and methods.

In fig 4a and 4b two selected approach and retract curves at low ($5\mu\text{m/s}$) and high indentation rate ($20\mu\text{m/s}$) are reported. The colored area between the approach and the retract curve provides a graphical representation of H .

As demonstrated in fig 1, a single point measure is not fully representative of the whole cell mechanical response. Therefore we calculated H by using maps of the same size and resolution as those used in fig 2. The average H value was then calculated for each map, taking into account only those pixels occupied by the erythrocyte and discarding those that correspond to the glass coverslip.

By increasing indentation rate, the average H undergoes a significant increase from about 17% at low indentation rate up to reach a plateau value of about 27% at $15\mu\text{m/s}$. Then it remains constant.

Comparative study of the mechanical response of normal and diabetes mellitus RBC.

Diabetes mellitus, one of the most debilitating conditions that our society suffers from, is a pathology closely related to

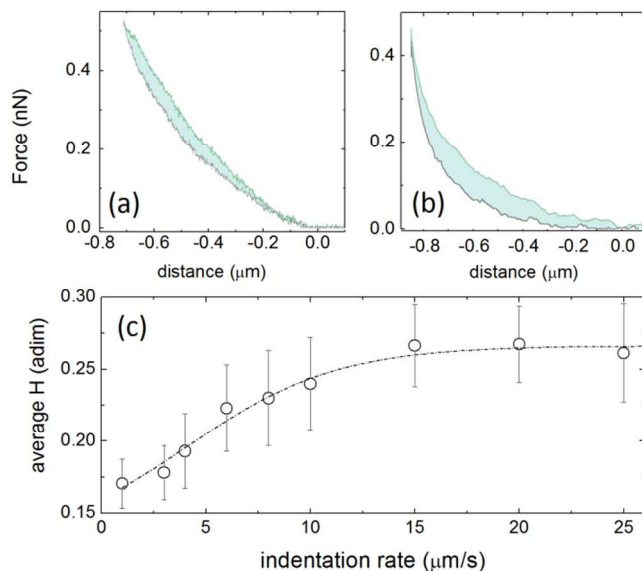


Figure 4: two selected approach and retract curves acquired at 5 μm/s (panel a) and 20 μm/s (panel b). The green area between the approach and the retract curves provides a graphical representation of the calculated hysteresis (H). Average H value as a function of the indentation rate (panel c). Error bars correspond to the standard deviation of the mean computed over all the measured cells.

to oxidative stress. Erythrocytes, in their turn, are particularly vulnerable to oxidative stress. In this regard it has been recently shown that red blood cells in diabetes have a significantly changed shape as well as a decreased membrane roughness³².

Aside from morphological modifications, several works reported that RBCs extracted from control subjects are softer than those extracted by patients suffering from diabetes mellitus. In these works indentation measurements have been performed by using a single indentation rate. However, as demonstrated in fig 2, the mechanical response of RBCs is strongly dependent on the indentation rate, as well as, on the indenting position within the cell surface.

In figure 5a, the behavior of the average apparent Young's Modulus E of RBCs extracted from patients suffering from diabetes mellitus is shown as a function of the indentation rate. Measurements (large open circles) were performed in the same fashion as done in fig 2 and were also compared to those reported in fig 2 (black dots). Three regimes can be clearly distinguished. At low indentation rate (1 μm/s), the measured average Young's modulus is about 1.8 kPa. This value is consistent with that measured on healthy RBCs in fig 2. By increasing the indentation rate, the average E

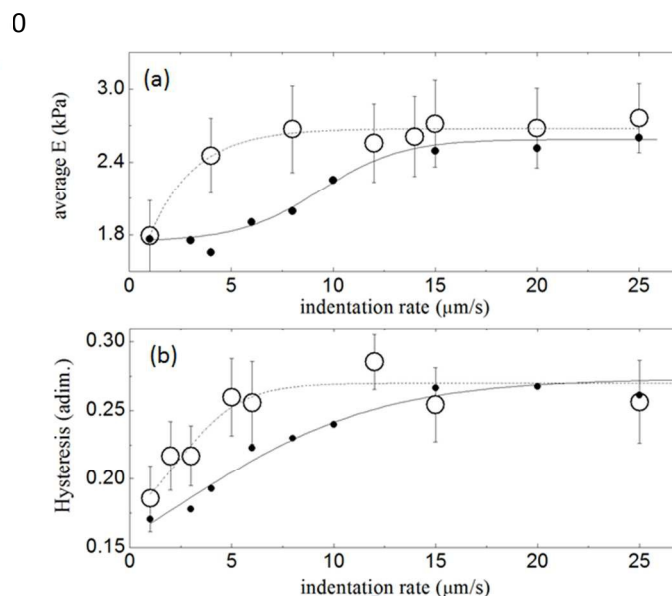


Figure 5: (panel a) average apparent Young's modulus E of RBCs extracted from diabetes mellitus patient as a function of the indentation rate (large open circle). Data are compared to those reported in fig 2 for healthy subjects (black dots). (Panel b) average Hysteresis H measured on the same sample as a function of the indentation rate (large open circles). Data are compared to those reported in fig. 4 for healthy subjects (black dots). For clarity error bars are not displayed.

undergoes an abrupt increase reaching a plateau value of about 2.5 KPa after 5 μm/s. One can observe that in the range between 2 μm/s and 10 μm/s, pathological RBCs are significantly stiffer than healthy ones. Notably, at high indentation rate, larger than 10 μm/s, both healthy and pathological red blood cells display similar values.

In fig 5b the average hysteresis measured on the same sample is reported as a function of the indentation rate (large open circles). Data are compared to those reported in fig 3

for a healthy subject. In this case also, at low indentation rate, the measured H value is similar for both samples. Then the pathological sample shows an abrupt increase of H , reaching a plateau value at about $5 \mu\text{m/s}$. Conversely, the healthy sample shows a smoother increase with respect to the pathological one. Notably, also in this case both samples reach similar plateau value.

Discussion

The onset and the progression of several diseases are known to induce significant changes in the geometrical and mechanical properties of RBCs, such as cell size, shape and deformability. However these modifications occurring at the whole cell level are closely related to changes in the molecular composition and organization of the cell that, in their turn, occur at the nanoscale. This has made it necessary to develop quantitative tools able to probe RBCs changes at nanometers and piconewton scales. In this context, the work of Girasole and coworkers pointed out a close relation between the presence of selected pathologies (and/or aging conditions) and the modifications of RBCs surface roughness as measured by AFM^{33, 34}. This study provides a direct proof that quantitative parameters measured at the nanoscale level have potential applications in the clinical practice as a diagnostic tool. This is further confirmed by the fact that roughness modifications are closely related to changes occurring at the spectrin network level³⁵.

Another key parameter having the potential to promote the development of novel diagnostic tools is Young's modulus as measured by AFM. Young's modulus, indeed, was proven to be effective in distinguishing between normal and pathological erythrocytes in several disease conditions. The translation of these results to the clinical practice is nowadays particularly straightforward thanks to the development of a new generation of fast-scan AFM set-ups that are able to significantly reduce typical AFM acquisition times.

One of the main factors still hindering a wide applicability of Young's modulus in the clinical practice depends on the fact that the measured RBCs stiffness may undergo large variations depending on cell preparation. This is clearly observable in tab. S1 (supplementary information) where a quantitative comparison between the average Young's

modulus measured in this paper and that measured in similar experimental papers is shown. It can be noted that AFM experiments performed on fixed cells provide an average E ranging between several tents to several hundred of kPa^{10, 11}. These values are significantly higher than those measured on unfixed cells, both dried or resuspended in buffer solution, that range between few hundreds of Pa¹³ to few kPa⁴.

In this work we measured an average E value of 1.82 ± 0.40 kPa with a standard deviation of 1.6 kPa obtained by the analysis of 15 healthy subjects. These values are very close to that measured in similar condition by Lamzin et al.¹² and Maciaskek et al.¹ that obtained, respectively, 1.81 ± 0.44 kPa and 1.1 ± 0.44 kPa. Moreover our data appear to be consistent with that measured by Brimmel and co-workers that range between 1.27 and 7.22 kPa⁸, and lower than that measured in ref⁴ that reported an average Young's modulus of 4.9 ± 0.5 kPa. As highlighted in tab S1, this discrepancy may be related to different cell preparation protocol.

As clearly pointed out in fig 1, the RBC mechanical response is not homogeneous over the cell body. Interestingly, E values show a cylindrical symmetry around the "z" axis. Moreover, by comparing fig. 1d and 1e, it appears that RBCs height and E values are anticorrelated: the higher the z -coordinate the lower the Young's Modulus. This result is particularly relevant for the long term debated problem of whether the cytoskeleton of a resting red blood cell is stress-free or under stress³⁶. Our results strongly suggest the latter hypothesis is more likely than the former. Moreover we feel that this result may positively impact on the theoretical modeling of red blood cells motion under a flowing condition, where it is necessary to make an assumption about the stress-free state³⁶⁻⁴¹.

In most of the biomechanics AFM studies, the basic assumption is that the RBC behaves like an elastic body: hence, dissipative forces are neglected and Young's modulus is treated as unaffected by probe dynamics. In this work we show that this assumption cannot be considered strictly valid. As indeed pointed out in fig 3, the apparent average RBC Young's Modulus shows a clear sigmoidal dependence on the indentation rate. This finding demonstrates that RBCs show a viscoelastic behavior. As recently demonstrated in the papers of Prado et al¹⁵ and Tomaiulo et al¹⁷. This behavior can be due both to the RBC membrane viscosity

η_m^{2D} and the internal viscosity η_{in} . By combining an advanced theoretical modeling and a microfluidic approach, Prado et al¹⁵ recently estimated membrane viscosity value of about $\sim 10^{-7} Nsm^{-1}$.

5 The sigmoidal behavior shown in fig 3 is in agreement with the “standard linear solid” (SLS) model, a three-parameters model using a linear combination of springs and dashpots to represent elastic and viscous components, respectively. This model consists of two systems in parallel. The first, referred
10 to as the Maxwell arm, contains a spring (K) and dashpot (viscosity η) in series; the other system contains only a spring k_e . As demonstrated in ref.⁴², the sample reaction force $F(z)$ can be expressed, under the boundary condition $F(z=0)=0$ and the assumption of constant indentation
15 velocity and as:

$$F(z) = k_e z + \eta v - \eta v e^{-\frac{Kz}{\eta v}} \quad (3)$$

According to the previous equation, the sample reaction
20 force at very low velocity is dominated by the pure elastic contribution $F(v \rightarrow 0) \sim k_e z$ whereas at high velocity by the plateau value, $F(v \rightarrow \infty) \sim (k_e + K)z$. In the intermediate velocity range, the viscosity contributes increasing the reaction force with the velocity, in a non-linear way, until
25 the reaction force reaches the plateau $F(v \rightarrow \infty) \sim (k_e + K)z$. The experimental sigmoidal behavior shown in fig 3 that starts from a lower plateau value then increasing in a nonlinear fashion up to reach a higher plateau value fits very well, from a qualitative point of view, the SLS model.

30 Moreover, under the assumption that adhesion forces can be neglected, also the normalized hysteresis value H shown in fig 4 is in a qualitative accordance with the standard solid model, increasing and reaching a plateau value at high indentation rates.

35 The key role played by viscous forces in the biomechanical response of red blood cells is further stressed by the comparison between the biomechanical response of normal and pathological cells. In both cases a strong dependence on the indentation rate can be observed. It is worth stressing
40 that most of AFM biomechanical studies concerning red blood cells are performed at a single constant indentation rate, usually in the range 2-10 $\mu m/s$. Interestingly, in this velocity range, we detected a 27% increase in the

pathological average Young’s modulus with the respect to
45 the healthy subjects. This increment is of the same order of that measured in ref⁴ that is about 43%. Conversely, out of this range normal and pathological red blood cells appears to have a similar biomechanical response. If considered in term of the above-mentioned SLS model, this finding
50 suggests that the viscous contribution plays a crucial role in determining the difference in the mechanical response.

Conclusions

In this work we probed the biomechanical response of red
55 blood cells by AFM nano-mapping. Our high-resolution maps acquired in physiological solution unveil the local changes in the cell elastic properties, demonstrating that healthy erythrocytes are stiffer in their center and softer at the cell periphery. The measured stiffness profile shows a
60 cylindrical symmetry that appears to be strongly correlated with the RBC biconcave shape. These results stress that a single point measure (as well as some random-landing measures) often used in AFM experiment, cannot be representative of the whole RBCs mechanical response.

65 The measured stiffness profile is also highly interesting for the long-term debated problem of whether the cytoskeleton of a resting red blood cell is stress-free or under stress⁴⁴, suggesting the latter hypothesis is more likely.

The viscoelastic behavior of healthy and pathological red
70 blood cells was also investigated by acquiring force distance-curves at different indentation rates. Our experiment shows a marked Young’s modulus dependence on the indentation rate providing compelling evidence that RBCs do not behave as a pure elastic body. Conversely
75 viscous forces, rarely considered in AFM experiments on RBCs, have a key role in determining their mechanical response. This finding is in close agreement with the results of Yoon and co-workers⁷. In this paper, the authors studied the dynamical biomechanical response of RBCs by optical
80 tweezers, showing a large stiffness increase with the increasing of the strain rate from 0.2 $\mu m/s$ to 20 $\mu m/s$.

The fundamental role of viscous forces is further stressed by the comparison between healthy and pathological red blood cells. Diabetes mellitus has been taken as a model system,
85 since red blood cells are known to be stiffer than normal ones. Our data provide a more complex scenario in which

pathological red blood cells are not simply stiffer than healthy ones. Conversely they might show a different dependence on the indentation rate that leads to an apparent increase in stiffness.

5 These results suggest that in pathological cases, not only the RBCs static deformation, but also their dynamic behavior could be affected. Interestingly, this observation fits very well with changes occurring in healthy red blood cells under in-vivo aging conditions. It is worth to note that, under these 10 conditions as well as the majority of pathological conditions, an increase in cells stiffness can be detected. Nash and Meiseleman demonstrated that membrane elastic modulus does not change during aging; conversely, the time constant for cell shape recovery undergoes large variations. This 15 behavior – in its turn - implies that a greater force is required to reach the RBC final deformation^{42, 43}. In all these cases a RBCs deformation delay, produced by dissipative internal forces, should be considered one of the main actors for the blood flow resistance in microvessels observed in several 20 pathologies. Finally, from a clinical point of view, we want to point out that novel machanobiological markers of diseases are currently based on the measure of the average RBC Young's modulus obtained at a constant indentation speed. Taken together our results show that both the local 25 stiffness distribution and the viscoelastic response not only provide important information on the RBC biomechanics but also can be more effective than the average Young's modulus in distinguishing between healthy and pathological red blood cells.

30

Acknowledgements

This research has been supported by Università Cattolica del Sacro Cuore of Rome. Measurements were performed at the 35 Laboratorio Centralizzato di Microscopia ottica ed elettronica facility (LABCEMI) of Università Cattolica del S. Cuore (Rome, Italy). We are extremely thankful to Mario Amici for the technical support in experiments. The authors declare no commercial or financial conflict of interest.

40

Notes and references

1 Istituto di Fisica, Università Cattolica del Sacro Cuore, Largo F. Vito 1, 00168, Roma, Italy.

45 2 Istituto di Biochimica e Biochimica Clinica, Università Cattolica del Sacro Cuore, Largo F. Vito 1, 00168, Roma, Italy.

*Corresponding author: m.papi@rm.unicatt.it

50

References

1. J. L. Maciaszek and G. Lykotrafitis, *J Biomech*, 2011, 44, 657-661.
2. M. Dao, C. T. Lim and S. Suresh, *Journal of the Mechanics and Physics of Solids*, 2003, 51, 2259-2280.
3. D. E. Discher and P. Carl, *Cell Mol Biol Lett*, 2001, 6, 593-606.
4. M. Lekka, M. Fornal, G. Pyka-Fosciak, K. Lebed, B. Wizner, T. Grodzicki and J. Styczen, *Biorheology*, 2005, 42, 307-317.
5. G. Lenormand, S. Henon, A. Richert, J. Simeon and F. Gallet, *Biorheology*, 2003, 40, 247-251.
6. C. T. Lim, M. Dao, S. Suresh, C. H. Sow and K. T. Chew, *Acta Materialia*, 2004, 52, 4065-4066.
- 65 7. Y. Yoon¹, J.Kotar, G. Yoon, P. Cicuti, *Phys. Biol.*2008, 5 art no. 036007
8. K. E. Bremmell, A. Evans and C. A. Prestidge, *Colloid Surface B*, 2006, 50, 43-48.
9. S. Chien, *Annual Review of Physiology*, 1987, 49, 177-192.
- 70 10. I. Dulinska, M. Targosz, W. Strojny, M. Lekka, P. Czuba, W. Balwierz and M. Szymonski, *Journal of Biochemical and Biophysical Methods*, 2006, 66, 1-11.
11. M. Girasole, S. Dinarelli and G. Boumis, *J Mol Recognit*, 2012, 25, 285-291.
- 75 12. I. M. Lamzin and R. M. Khayrullin, *Anat Res Int*, 2014, 2014, 869683.
13. M. Li, L. Q. Liu, N. Xi, Y. C. Wang, Z. L. Dong, X. B. Xiao and W. J. Zhang, *Sci China Life Sci*, 2012, 55, 968-973.
- 80 14. H. Noguchi and G. Gompper, *Proceedings of the National Academy of Sciences of the United States of America*, 2005, 102, 14159-14164.
15. G. Prado, A. Farutin, C. Misbah and L. Bureau, *Biophys J*, 2015, 108, 2126-2136.
- 85 16. L. Lanotte, G. Tomaiuolo, C. Misbah, L. Bureau, S. Guido, *Biomicrofluidics*, 2014, 8 art. no. 014104. doi 10.1063/1.4863723
17. G. Tomaiuolo and S. Guido, *Microvasc Res*, 2011, 82, 35-41.
- 90 18. Y. Zheng, J. Chen, T. Cui, N. Shehata, C. Wang and Y. Sun, *Lab on a Chip*, 2014, 14, 577-583.
19. Y. Zheng, E. Shojaei-Baghini, A. Azad, C. Wang and Y. Sun, *Lab on a Chip*, 2012, 12, 2560-2567.
- 95 20. E. Pretorius and D. B. Kell, *Integrative Biology*, 2014, 6, 486-510.
21. P. De Sole, C. Rossi, M. Chiarotto, G. Ciasca, B. Bocca, A. Alimonti, A. Bizzarro, C. Rossi and C. Masullo, *Clin Biochem*, 2013, 46, 89-93.
- 100 22. M. Fornal, M. Lekka, G. Pyka-Fosciak, K. Lebed, T. Grodzicki, B. Wizner and J. Styczen, *Clinical*

- Hemorheology and Microcirculation*, 2006, 35, 273-276.
23. B. J. Briscoe, K. S. Sebastian and M. J. Adams, *Journal of Physics D-Applied Physics*, 1994, 27, 1156-1162.
- 5 24. I. N. Sneddon, *International Journal of Engineering Science*, 1965, 3, 47-57.
25. A. Boccaccio, M. C. Frassanito, L. Lamberti, R. Brunelli, G. Maulucci, M. Monaci, M. Papi, C. Pappalettere, T. Parasassi, L. Sylla, F. Ursini and M. De Spirito, *J R Soc Interface*, 2012, 9, 2871-2882.
- 10 26. A. Boccaccio, L. Lamberti, M. Papi, M. De Spirito, C. Douet, G. Goudet and C. Pappalettere, *Interface Focus*, 2014, 4.
27. M. Papi, P. Paoletti, B. Geraghty, R. Akthar, *Appl Phys Lett*, 2014, 104 (10), art. no. 103703.
- 15 28. V. Palmieri, D. Lucchetti, A. Maiorana, M. Chiarpotto, G. Maulucci, M. Papi, G. Ciasca, A. Sgambato and M. De Sprito, *Soft Matter*, 2015, 11, 5719-5726.
29. V. Palmieri, D. Lucchetti, A. Maiorana, M. Papi, G. Maulucci, G. Ciasca, M. Svelto, M. De Spirito and A. Sgambato, *Appl Phys Lett*, 2014, 105, art. no. 123701
- 20 30. C. R. A. Berquand, S. Kasas, A. Holloschi, L. Ponce, M. Hafner, 2010, *Microscopy Today*, 8.
31. M. Papi, A. Maiorana, C. Douet, G. Maulucci, T. Parasassi, R. Brunelli, G. Goudet and M. De Spirito, *Appl Phys Lett*, 2013, 102, art. no. 043703
- 25 32. A. V. Buys, M. J. Van Rooy, P. Soma, D. Van Pependorp, B. Lipinski and E. Pretorius, *Cardiovascular Diabetology*, 2013, 12.
- 30 33. M. Girasole, G. Pompeo, A. Cricenti, A. Congiu-Castellano, F. Andreola, A. Serafino, B. H. Frazer, G. Boumis and G. Amiconi, *Bba-Biomembranes*, 2007, 1768, 1268-1276.
34. M. Girasole, G. Pompeo, A. Cricenti, G. Longo, G. Boumis, A. Bellelli and S. Amiconi, *Nanomedicine-Nanotechnology Biology and Medicine*, 2010, 6, 760-768.
- 35 35. L. Picas, F. Rico, M. Deforet and S. Scheuring, *Acs Nano*, 2013, 7, 1054-1063.
- 40 36. D. Cordasco, A. Yazdani and P. Bagchi, *Phys Fluids*, 2014, 26.
37. T. Kruger, D. Holmes and P. V. Coveney, *Biomicrofluidics*, 2014, 8.
38. T. Svelc and S. Svetina, *Cell Mol Biol Lett*, 2012, 17, 217-227.
- 45 39. D. Xu, E. Kaliviotis, A. Munjiza, E. Avital, C. N. Ji and J. Williams, *J Biomech*, 2013, 46, 1810-1817.
40. D. E. Discher, D. H. Boal and S. K. Boey, *Biophys J*, 1998, 75, 1584-1597.
- 50 41. X. J. Li, Z. L. Peng, H. Lei, M. Dao and G. E. Karniadakis, *Philos T R Soc A*, 2014, 372.
42. J. Schmitz, M. Benoit and K. E. Gottschalk, *Biophys J*, 2008, 95, 1448-1459.
43. G. B. Nash and H. J. Meiselman, *Biophys J*, 1983, 43, 63-73.
- 55 44. D. Cordasco, A. Yazdani, P. Bagchi *Physics of Fluids*, 2014, 26, art no. 041902